JOURNAL OF THERMOPHYSICS AND HEAT TRANSFER
Vol. 14, No. 2, April–June 2000

Film Cooling Measurements on Cylindrical Models with Simulated Thermal Barrier Coating Spallation

S. V. Ekkad*
Louisiana State University, Baton Rouge, Louisiana 70803
and
J. C. Han†
Texas A&M University, College Station, Texas 77843

Detailed heat transfer coefficient and film effectiveness distributions are presented on a cylindrical leading-edge model with simulated thermal barrier coating spallation using a transient liquid crystal technique. Tests were performed in a low-speed wind tunnel on a cylindrical model in a crossflow with two rows of injection holes. Mainstream Reynolds number based on the cylinder diameter was 1.009×10^5. The two rows of injection holes were ± 15 deg from stagnation. The film holes were spaced four hole diameters apart and were angled 30 and 90 deg to the surface in the spanwise and streamwise directions, respectively. The simulated spallation cavities were rectangular in shape and had rounded edges. The simulated spallation was placed at two locations, 20–40 deg (S3) and 35–55 deg (S4), respectively. The cylinder surface was coated with thermochromic liquid crystals, and a transient test was run to obtain the heat transfer coefficients and film effectiveness. The effect of coolant blowing ratio was studied for blowing ratios of 0.4 and 0.8. Results show that the Nusselt numbers increase and film effectiveness values decrease with an increasing blowing ratio. An increase in freestream turbulence has a very little effect on Nusselt numbers but reduces the film effectiveness significantly at low blowing ratios. In general, presence of spallation enhances Nusselt numbers and produces a strong variation in film effectiveness distributions.

Nomenclature

b	= bar grid width
D	= cylinder model diameter
h	= heat transfer coefficient
k	= thermal conductivity of test surface
k_{air}	= thermal conductivity of mainstream air
M	= blowing ratio ($\rho_c U_c / \rho_\infty U_\infty$)
Nu	= Nusselt number based on cylinder diameter, hD/k_{air}
Re	= Reynolds number based on incident mainstream velocity, $U_\infty D/\nu$
T_i	= initial temperature of test surface
Tu	= streamwise turbulence intensity, $\sqrt{(\bar{u}'^2)}/U_\infty$
T_w	= liquid crystal red–green color change temperature
T_∞	= mainstream temperature
t	= time for liquid crystal color change
U_c	= local velocity of coolant
U_∞	= incident mainstream velocity
u'	= fluctuating velocity
X	= axial distance from the grid location
α	= thermal diffusivity of test material
η	= film effectiveness
θ	= angle from stagnation
ρ_c	= density of coolant
ρ_∞	= density of mainstream

Introduction

HIGHER inlet temperatures in modern gas turbine engines provide higher power output and higher thermal efficiency. High-temperature gases have a damaging effect on the engine components that are in the hot gas path. Thermal barrier coatings (TBC) are often used to protect engine component metal surfaces from these high-temperature gases. The metal surface is coated by spraying a thin layer of high-temperature resistant TBC material. Power generation turbines typically use coal-derived fuels to economize the power production. With the use of coal-derived fuels, the TBC surface undergoes severe thermal stresses, erosion, and corrosion during the engine operation. These stresses cause the TBC layer to peel and expose the inner metal surface. The peeling of TBC layer due to exposure to extremely harsh environments produces a spallation. Spallation leads to a loss of thermal protection of the inner metal surface. This could result in a rapid failure of the exposed engine components and penalize the overall efficiency and life of the entire gas turbine engine. The rapid failure results from the loss of thermal protection and enhancement of heat transfer coefficients due to spallation. The enhanced heat transfer coefficients increase the heat loads around the spallation that is detrimental to the life of the component. The present study focuses on the effect of simulated TBC spallation with film cooling on the leading-edge region of a turbine blade.

In modern gas turbine engines, both film cooled and non-film-cooled blades utilize TBC to protect the blade material. TBC spallation also can occur on a film-cooled blade. Watt et al.[1] and Abuaf et al.[2] provide a detailed description of the TBC application process. Watt et al.[1] focused on the boundary-layer characteristics and losses due to the TBC layer, whereas Abuaf et al.[2] studied the stagnation heat transfer on a cylindrical leading model with real TBC. However, the literature presently lacks information on the effect of TBC spallation on film effectiveness and heat transfer coefficients. That TBC spalding can occur at random and that there is no defined shape or size of the spall make it difficult to analyze the actual spallation phenomena occurring on a real turbine blade. Thus, it needs to be modeled with predefined shape, size, and location to understand its effect on local heat transfer coefficients and film effectiveness. Ekkad and Han[3] studied the effect of cavity shape, size, and depth on heat transfer enhancement over a flat surface. Their study correlated the effects of various geometrical parameters of such simulated spallation cavities on heat transfer. They presented detailed heat transfer enhancement distributions using a transient liquid crystal technique. Ekkad and Han[4] studied the effect of simulated TBC spallation on a cylindrical leading-edge model of a non-film-cooled blade. Detailed

Received 10 May 1999; revision received 1 November 1999; accepted for publication 12 November 1999. Copyright © 2000 by the American Institute of Aeronautics and Astronautics, Inc. All rights reserved.

*Assistant Professor, Mechanical Engineering Department. Member AIAA.
†Heat Transfer Research Institute Professor, Department of Mechanical Engineering. Associate Fellow AIAA.

heat transfer coefficient distributions were obtained in their studies using a transient liquid crystal imaging method. They reported that the surface heat transfer coefficients can be enhanced up to two times in the presence of spallation compared to that for the surface without film cooling and spallation. The depth of the spallation cavity also has a strong effect on the local heat transfer coefficients. They further reported that the freestream turbulence increases the local heat transfer coefficients over the entire surface.

The leading edge region of the turbine blade has been a focus of many heat transfer studies. O'Brien and Van Fossen[5] and Morehouse and Simoneau[6] studied the effect of freestream turbulence on the forward-half of a circular cylinder. Bellows and Mayle[7] and Mehendale et al.[8] studied heat transfer on a simulated semicircular leading edge with a flat afterbody. They reported that an increase in the freestream turbulence intensity increases the leading-edge heat transfer significantly. All of the cited studies were for a test surface with no roughness or film-cooling effects.

Film cooling on the leading edge has also been a focus of several investigations. Mick and Mayle[9] studied film cooling on a blunt body with a semicircular leading edge and a flat afterbody. Their results showed that the surface heat loads reduce at low blowing ratios. They also determined that the high effectiveness regions do not necessarily correspond with the regions having high heat transfer coefficients. Mehendale and Han[10] studied the effect of freestream turbulence on leading-edge film-cooling effectiveness and heat transfer coefficients. They reported that the heat transfer coefficients increase with an increase in turbulence levels and that the film effectiveness reduces. Ou et al.[11] studied the effect of film hole row location on a test model similiar to that of Mehendale and Han.[10] Their results show that the effectiveness was higher for the hole row farther downstream of stagnation. Ekkad et al.[12] used a transient liquid crystal imaging method to obtain detailed heat transfer coefficients and film effectiveness on a cylindrical leading-edge model. Their results indicate that for air injection (density ratio = 1.0) heat transfer coefficients increase with increase in blowing ratio. The best effectiveness is obtained at a blowing ratio of 0.4 for air injection. They also reported that the freestream turbulence has little effect in heat transfer enhancement but is detrimental to film effectiveness.

The present study simulates the effect of TBC spallation on a cylindrical leading-edge model of a film-cooled blade. Detailed heat transfer coefficients and film effectiveness is measured using a transient liquid crystal imaging technique. In this study, spallations downstream of the film hole row are studied. Two different depths of spallation are simulated to understand the effect of depth. The simulated spallation model has a rectangular shape with rounded edges and is similar to the spallations that typically occur on the turbine blade.

Experimental Setup

A schematic of the test facility is shown in Fig. 1. The facility consists of a suction-type blower at the downstream end of the test tunnel and a 3:1 contraction nozzle upstream of the test tunnel. The test tunnel is 25.4 × 76.2 cm and is 183 cm long. The test cylinder is placed 77.5 cm downstream of the nozzle exit. A tailboard is placed at the rear of the test cylinder to reduce wake effects on the upstream heat transfer. The image processing system is used for measuring the detailed heat transfer and film effectiveness distributions. The imaging system consists of a red–green–blue (RGB) camera, monitor, and a personal computer with color frame grabber board. A turbulence grid is placed between the nozzle and the test section inlet to generate a higher turbulence level of 7.1%. The coolant flow loop is also shown in Fig. 1. Compressed air is routed through an orifice meter for the coolant flow. The coolant is initially directed away from the test cylinder through a three-way diverter valve. The valve is switched as the transient test is initiated. An inline heater, housed in the coolant supply line, is used to heat the coolant flow for the film effectiveness tests.

Figure 2 shows the test cylinder. The cylinder is 7.62 cm in diameter and 25.4 cm high. The cylinder has a black polycarbonate exterior and a hollow copper interior. Six cartridge-type heaters 0.32 cm in diameter and 25.4 cm in length are embedded in the copper interior along the circumference to heat the cylinder uniformly. The polycarbonate exterior is mounted over the copper interior such that there is always a good thermal contact between the two. This ensures uniform heating of the polycarbonate exterior. The polycarbonate exterior is 0.64 cm thick and has a very low thermal conductivity

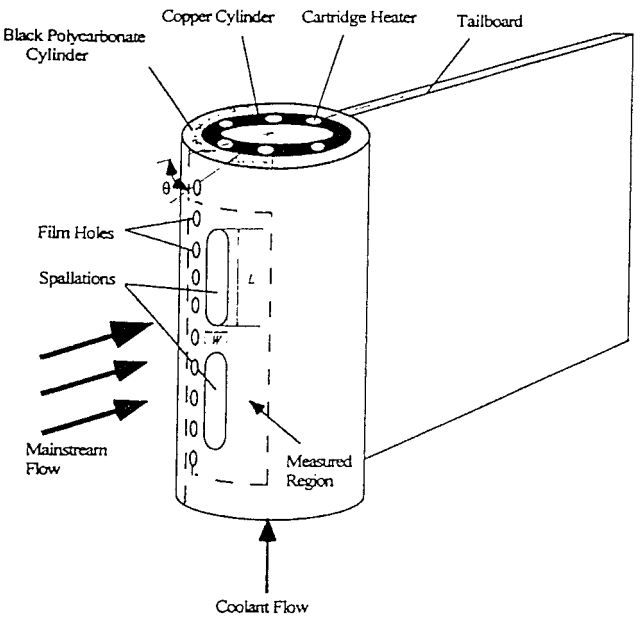

Fig. 2 Cylindrical leading-edge test model.

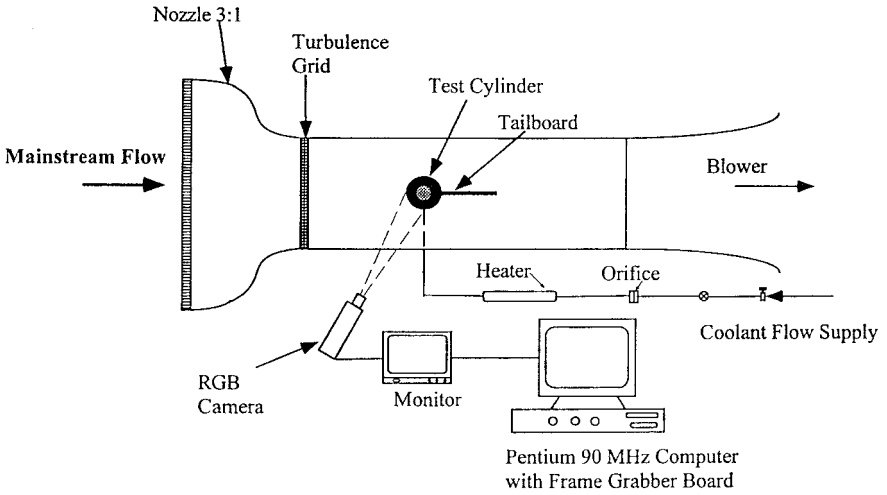

Fig. 1 Experimental test facility.

and diffusivity. Film holes are drilled through the copper and polycarbonate layers. The coolant is sent to the hollow inside of the test cylinder and is ejected out of the film holes. The film holes, placed at ±15 deg from the leading edge, are 0.475 cm in diameter and are inclined 30 and 90 deg in the spanwise and streamwise directions, respectively. In each row, 10 holes are spaced four hole diameters apart ($P/d = 4$). The film hole-to-diameterratio (d/D) was 0.063, and the film hole length-to-diameterratio was 3.1. The simulated spallation cavities are machined on the polycarbonate exterior downstream of the film hole row. The polycarbonate exterior can be also changed for different spallation locations. Two models are made for two different spallation locations. Each spallation occupies about 20-deg width on the cylinder surface. Spallations are placed at 20–40 deg (S3) and 35–55 deg (S4). Two different spallation depths of 0.25 and 0.51 cm are tested for each spallation location. The real spallation is similar to the slot shape that is simulated in this study. The thickness of the spall on the real engine blade is in the range of 0.5–1.2 μm. The mainstream flow velocity is very low compared to that in the engine. Thus, to simulate the Reynolds number around the leading-edge region, the leading-edge model has to be enlarged. The spallation geometry is, therefore, accordingly scaled up. The measurement region shown in Fig. 2 is limited to one side of the front-half of the cylinder from stagnation (0 deg) to 70 deg from stagnation. The test model is symmetrical and only front-half of the cylinder is used for measurement for a single configuration.

The test surface is sprayed uniformly with thermochromic liquid crystals. Liquid crystal color change temperatures for the appearance of red, green, and blue were 31.6, 32.7, and 37.2°C, respectively. The test surface is heated uniformly using the cartridge heater to a temperature above the liquid crystal color change temperature range. Several thermocouples are placed on the surface of the test cylinder to monitor the surface temperature. In the present experiment, the surface of the test cylinder is heated to a temperature above the temperature corresponding to the blue color. The test surface is suddenly cooled by inducing the mainstream flow by the fast starting blower. The blower takes less than 3 s from initiation to full flow rate. The liquid crystal color changes from blue to green, then to red, then to colorless during the transient test. The coolant flow is initiated by the solenoid controlled three-way diverter valve. The frame grabber board and the personal computer are used for real-time image capture and analysis. The data are stored in a file that is postprocessed to obtain heat transfer and film effectiveness values.

Data Analysis

For the case without film cooling, heat transfer coefficients for the leading-edge model with and without spallation can be obtained as follows. A one-dimensional conduction into a semi-infinite surface with a convective boundary condition at the surface is assumed. The surface temperature response is described by the solution

$$(T_w - T_i)/(T_\infty - T_i) = 1 - \exp(h^2\alpha t/k^2)\,\mathrm{erfc}(h\sqrt{\alpha t}/k) \quad (1)$$

where T_w is the temperature for green-to-red transition of liquid crystal color change during transient cooling. The time t for the actual appearance of red at any location on the test surface is measured during the transient test. The thermal conductivity k and diffusivity α of the test material are known. The local heat transfer coefficient h at any location on the test surface can be obtained from Eq. (1).

For film-cooling tests, the mainstream temperature T_∞ in Eq. (1) is replaced by the local film temperature T_f, which is a mixture of the coolant temperature T_c and mainstream temperature. To find the unknown T_f with known T_∞ and T_c, a nondimensional temperature that is film-cooling effectiveness η is introduced as follows:

$$\eta = (T_f - T_\infty)/(T_c - T_\infty) \qquad \text{or} \qquad T_f = \eta T_c + (1-\eta)T_\infty \quad (2)$$

Replacing the T_∞ in Eq. (1) by T_f from Eq. (2), we get he following equation with two unknowns h and η:

$$T_w - T_i = [1 - \exp(h^2\alpha t/k^2)\,\mathrm{erfc}(h\sqrt{\alpha t}/k)][\eta T_c + (1-\eta)T_\infty - T_i] \quad (3)$$

Running two similar transient tests is, therefore, necessary to obtain the heat transfer coefficients h and the film effectiveness η. The two tests can be run with two different coolant temperatures. In the first test, T_c is nearly the same as T_∞ and, thus, T_f is equal to T_∞ and Eq. (1) can be used to calculate the heat transfer coefficients. For the second test, the coolant flow is heated to a temperature close to the initial temperature of the test surface. Film effectiveness is then obtained by rearranging Eq. (3) in the following manner:

$$\eta = \frac{T_w - T_{i_2}}{T_{c_2} - T_{\infty_2}}\frac{1}{F(h)} + \frac{T_{i_2} - T_{\infty_2}}{T_{c_2} - T_{\infty_2}} \quad (4)$$

where

$$F(h) = 1 - \exp(h^2\alpha t_2/k^2)\,\mathrm{erfc}(h\sqrt{\alpha t_2}/k)$$

where subscript 2 indicates the second test. The heat transfer coefficient h is obtained from the first test for the same experimental conditions. The duration of each test is a maximum of 60 s, which helps maintain the semi-infinite solid model assumption on the test surface.

Average experimental uncertainty in heat transfer coefficient and film effectiveness measurement is estimated to be about ±4.5 and ±6.8%, respectively. The individual uncertainties in color change time t is ±0.5 s, mainstream temperature T_∞ is ±0.2°C, coolant temperature T_c is ±0.2°C, surface initial temperature T_i is ±0.5°C, and material properties ($\sqrt{\alpha}/k$) is ±3%. Note that the uncertainty in the immediate vicinity of the film holes or edges of the cavity could be as high as ±17%. The preceding estimated levels could be caused by the two-dimensional conduction effects in these areas. The uncertainties have been estimated using the methodology of Kline and McClintock.[13]

Results and Discussion

Tests were conducted in a low-speed wind tunnel for a Reynolds number of 1.009×10^5 based on the cylinder diameter. Mainstream inlet velocities and densities are used to evaluate the blowing ratios. Air is used as a coolant so that the simulated density ratio is unity. Heat transfer results on the surface with film cooling and spallation and film cooling for two different turbulence intensities (1.0 and 7.1%) are presented. Heat transfer results with simulated spallation only are also presented for $Tu = 1$ and 7.1%. Two different blowing ratios ($M = 0.4$ and 0.8) were used for tests with film cooling. The film holes are located at ±15 deg from the stagnation. Two spallation locations, S3 (20–40 deg) and S4 (35–55 deg), were tested in conjunction with the film-injection holes.

The coolant-to-mainstream density ratios for the heat transfer coefficient and film effectiveness tests are almost equal. The heat transfer tests are run with both mainstream and coolant at room temperature, whereas in the film effectiveness tests the coolant is slightly hotter ($T_c \approx T_i$). Such a small difference in temperatures does not produce any significant variation in density ratios for the two tests.

Velocity and turbulence intensities were measured in the streamwise direction. Incident mainstream velocity U_∞ was obtained to be 21 m/s at $X/D = 9.5$ from the grid location. Streamwise turbulence decays rapidly downstream of the grid and reaches a low just upstream of the cylinder. This value is defined as the oncoming freestream turbulence intensity and is found to be 1% in the no-grid case and 7.1% with the grid. The corresponding streamwise dissipation length scale was found to be 1.5 cm for the grid-generated turbulence case. More details are presented on the turbulence generation in the study by Ekkad et al.[12]

Heat transfer coefficients were measured on the leading-edge model without film holes and spallations for the two turbulence levels. The local Nusselt number is normalized by the mainstream Reynolds number and the results are plotted as $Nu/Re^{0.5}$. The viscosity and the conductivity used to evaluate the $Nu/Re^{0.5}$ are based on the oncoming mainstream inlet flow. The results are discussed in detail by Ekkad et al.[12]

Heat Transfer Results

Figure 3 shows the effect of spallation location on the detailed $Nu/Re^{0.5}$ distributions with film cooling at a blowing ratio of $M =$

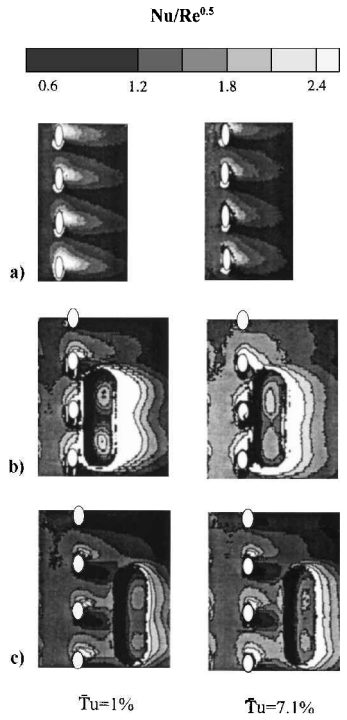

Fig. 3 At $M = 0.4$, detailed $Nu/Re^{0.5}$ distributions for a) film cooling only, b) film cooling and spallation S3, and c) film cooling and spallation S4.

0.4. Results for two freestream turbulence intensities of 1 and 7.1% are presented. For the cases without spallation and only film cooling, the increase in turbulence intensity has little effect on the $Nu/Re^{0.5}$ distributions. Results show that the film-cooling jets are more disturbed by S3 than S4. The spallation S3 enhances the local $Nu/Re^{0.5}$ values greatly downstream of the spallation. However, $Nu/Re^{0.5}$ values inside the spallation are lower compared to the surface with film cooling only. The film-cooling jets seem to separate at the upstream edge of the spallation cavity and reattach immediately downstream of the spallation. For the S4 case, the coolant jets are weaker as the spallation location S4 is farther downstream of the film-injection location. Thus, the effect of location S4 is smaller compared to that of S3. Higher $Nu/Re^{0.5}$ values are observed for higher freestream turbulence case. Higher freestream turbulence also increases local $Nu/Re^{0.5}$ values inside the spallation.

Figure 4 shows the spanwise-averaged Nusselt numbers ($Nu/Re^{0.5}$) for film cooling (Fig. 4a), film cooling and spallation S3 (Fig. 4b), and film cooling and spallation S4 (Fig. 4c) cases. Effect of blowing ratio ($M = 0.4$ and 0.8), spallation location, and turbulence intensity on heat transfer enhancement are presented. The presence of spallation increases the $Nu/Re^{0.5}$ values downstream and decreases $Nu/Re^{0.5}$ values inside the cavity. The film cooling without spallation for each turbulence intensity and blowing ratio is shown to indicate the enhancement caused by the spallation with film injection. Results for the surface without film cooling and spallation results are also plotted for comparison.

Effect of Blowing Ratio

$Nu/Re^{0.5}$ values increase with an increase in blowing ratio for all cases (Fig. 4). This is attributed to increased mixing caused by the

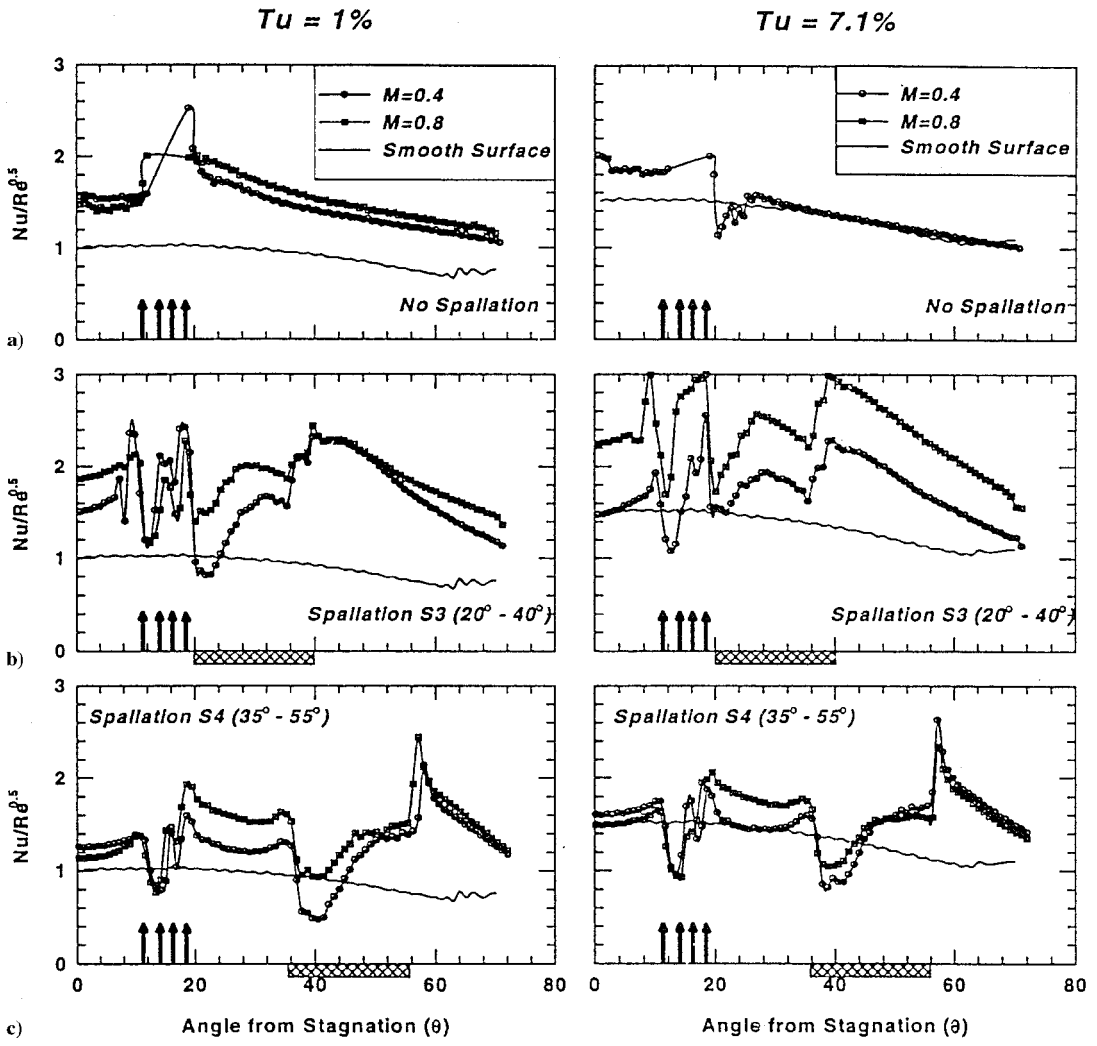

Fig. 4 Spanwise-averaged $Nu/Re^{0.5}$ for a) film cooling only, b) film cooling and spallation S3, and c) film cooling and spallation S4.

jet–freestream interactions. For the low-turbulence case, film cooling at both blowing ratios increase $Nu/Re^{0.5}$ values significantly over the leading-edge model without film cooling and spallation. $Nu/Re^{0.5}$ values are further enhanced in the presence of spallation downstream of the film-cooling hole row. In general, because higher blowing ratios cause stronger disturbances in the flow and, thus, enhance local turbulent mixing, this results in an increase in $Nu/Re^{0.5}$ values downstream of film-cooling hole row.

Effect of Spallation Location

Figures 4b and 4c show the effect of spallation and location of spallation on $Nu/Re^{0.5}$ values with film cooling. The presence of spallation downstream of the film-cooling hole row causes the film-cooling jets to detach from the surface at the upstream edge of the spallation cavity and to reattach immediately downstream. Inside the cavity, $Nu/Re^{0.5}$ values are lower compared to $Nu/Re^{0.5}$ values outside of the cavity. Because of the flow separation, the heat transfer coefficients are very low immediately downstream of the upstream edge of the spallation cavity. $Nu/Re^{0.5}$ value increases downstream as the flow reattaches inside the cavity near the downstream edge of the spallation cavity. When the spallation is placed immediately downstream of the film-cooling hole row (S3 case), the film-cooling jets show a strong interaction with the cavity and separate almost immediately. For a low blowing ratio ($M = 0.4$) the $Nu/Re^{0.5}$ values are even lower than the surface without film cooling and spallation $Nu/Re^{0.5}$ values in the region near the upstream edge of the spallation cavity. This may be because, at low blowing ratio, the low momentum coolant fluid remains closer to the surface and is trapped in the recirculation zone near the upstream edge of the cavity. However, for the $M = 0.8$ case, the $Nu/Re^{0.5}$ values are much lower because higher momentum coolant jets penetrate deeper into the mainstream and, thus, result in stronger mixing near the upstream edge of the spallation cavity. $Nu/Re^{0.5}$ values increase rapidly as the flow reattaches inside the cavity farther downstream of the upstream edge of the cavity. The flow again is tripped at the downstream edge and results in a new boundary layer, causing higher Nusselt number values downstream of the spallation.

When the spallation is placed farther downstream of the film-cooling hole row (S4 case), a similar separation and reattachment pattern is observed. However, because S4 is far away from the film-cooling hole row, its effect on $Nu/Re^{0.5}$ values may not be significant. The coolant jet–mainstream interactions may be much weaker nearer the spallation location S4. There are no results presented on flow distributions to confirm the jet–mainstream interactions.

Effect of Freestream Turbulence

An increase in turbulence intensity produces an increase in the $Nu/Re^{0.5}$ values for all cases. For the film-cooling only case, for $Tu = 7.1\%$, very little increase in the values of $Nu/Re^{0.5}$ is observed compared to values for the surface without film cooling and spallation under the same turbulence conditions. For the S3 case, under high freestream turbulence ($Tu = 7.1\%$), Nusselt numbers are enhanced almost two times compared to that for the surface without film holes and spallations. By the comparing of the low freestream turbulence ($Tu = 1\%$) case with high freestream turbulence case ($Tu = 7.1\%$), it is seen that, for low blowing ratio ($M = 0.4$), the heat transfer coefficients do not increase very significantly for all cases. This could be because film-cooling jets produce local disturbances in the flow near the wall that may have a predominant effect on local $Nu/Re^{0.5}$ values. For high blowing ratio ($M = 0.8$), increased interaction with the oncoming mainstream flow produces higher local turbulence levels and, hence, an increase in Nusselt number values (Fig. 4a). A similar trend can be observed for the higher blowing ratio. The heat transfer coefficients increase slightly for both S3 and S4 cases for the high turbulence case compared to low freestream turbulence case. However, an increase in freestream turbulence increases the $Nu/Re^{0.5}$ values inside the spallation cavity for both locations (Figs. 4b and 4c).

Film-Cooling Effectiveness Results

Figure 5 shows the effect of spallation location on detailed film effectiveness η distributions with film cooling at a blowing ratio of

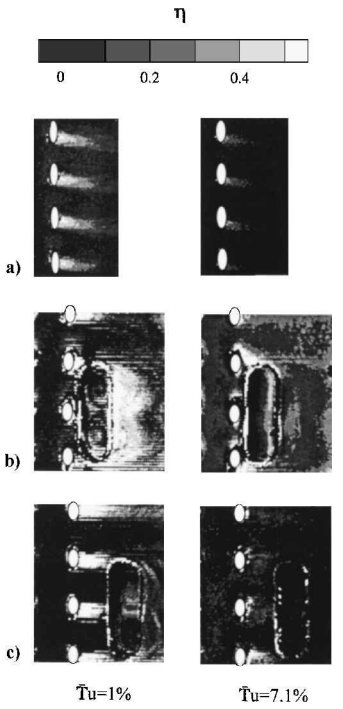

Fig. 5 At $M = 0.4$, detailed film cooling effectiveness η distributions for a) film cooling only, b) film cooling and spallation S3, and c) film cooling and spallation S4.

$M = 0.4$. The effectiveness distributions are jetlike along the film injection hole for the case without spallation at 1% turbulence intensity. For the case with S3 spallation, the jetlike pattern disappears, and the jets seem to coalesce immediately downstream of the spallation cavity. A high effectiveness region is observed downstream of location S3. This may be due to the jet separation and reattachment along the edges of the spallation cavity. The film effectiveness for the S4 case is similar compared to the case with only film cooling but only until the upstream edge of the spallation. For both spallation cases, film effectiveness is very low inside the spallation cavity. Higher freestream turbulence reduces the film effectiveness values for all cases. The jet structure breaks down under the influence of high freestream turbulence, thus reducing film effectiveness.

Figure 6 shows the spanwise averaged film effectiveness for the film cooling only (Fig. 6a), the film cooling and spallation S3 (Fig. 6b), and the film cooling and spallation S4 (Fig. 6c) cases. The effects of blowing ratio ($M = 0.4$ and 0.8), spallation location, and turbulence intensity on film effectiveness are presented. The presence of spallation increases the film effectiveness downstream and decreases the film effectiveness inside the spallation. In general, film effectiveness for the S3 case is higher than the S4 case. Film effectiveness decreases as the blowing ratio increases from $M = 0.4$ to 0.8.

Effect of Blowing Ratio

Under low freestream turbulence conditions ($Tu = 1\%$), blowing ratio of 0.4 shows higher film effectiveness for all cases. For the $M = 0.8$ case, the film-cooling jet still maintains its coherence and penetrates deeper into the mainstream flow. Thus, its effect near the wall is not as strong compared to low blowing ratio case. For the film-cooling-only case, film effectiveness is higher for $M = 0.4$ downstream of the film-cooling hole row. For the film-cooling and S3 case, downstream film effectiveness values are considerably larger for a lower blowing ratio. For the film-cooling and S4 case, similar trends are observed, although film effectiveness values are not as high as those for the film cooling and S3 case. However, the reverse is true for the high freestream turbulence condition ($Tu = 7.1\%$). At higher turbulence intensity ($Tu = 7.1\%$), for $M = 0.4$, the film-cooling jet is rapidly dissipated, and the film effectiveness is almost negligible for the film-cooling-only case. For the film-cooling and S3 case, film effectiveness for $M = 0.8$ is higher because the film-cooling

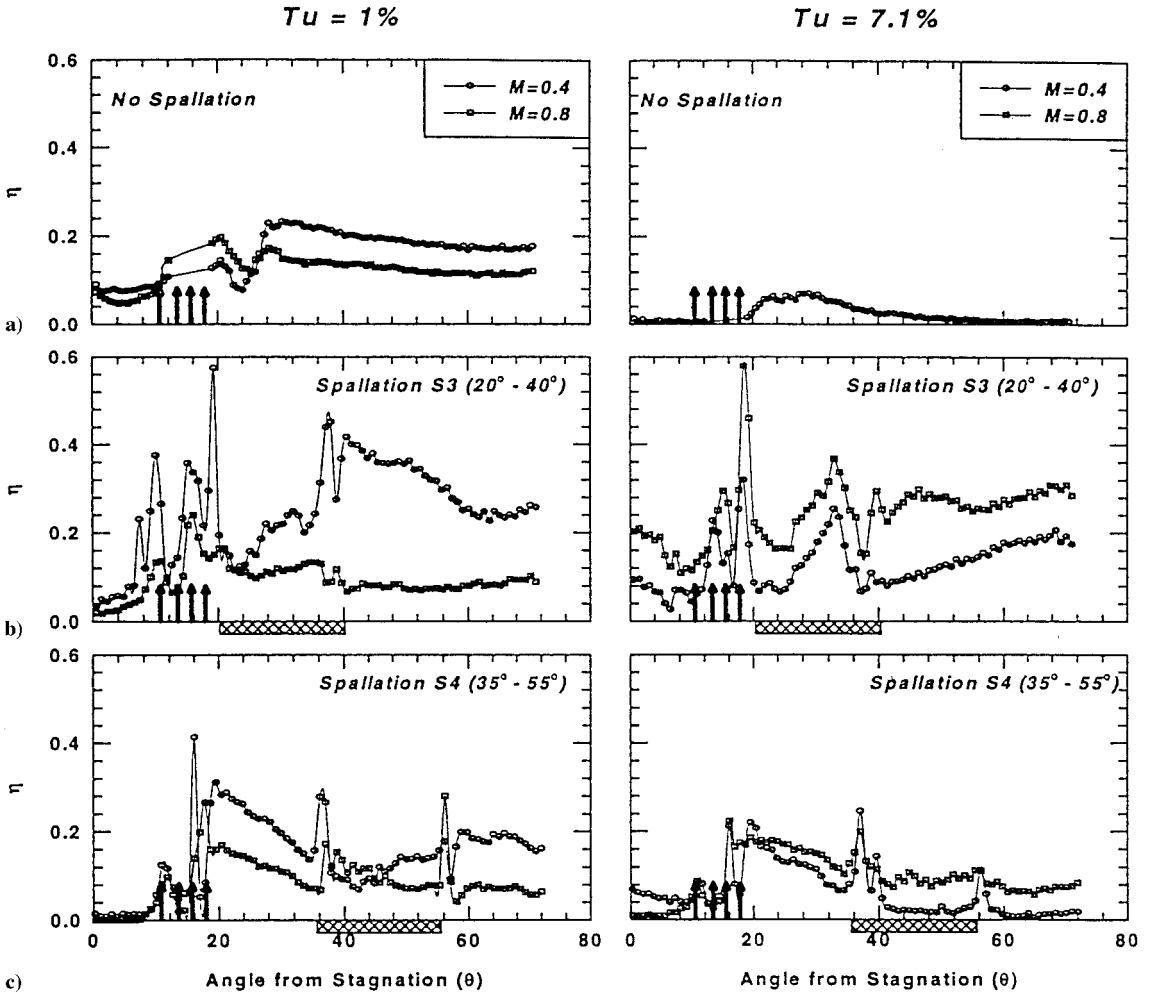

Fig. 6 Spanwise-averaged film cooling effectiveness η for a) film cooling only, b) film cooling and spallation S3, and c) film cooling and spallation S4.

jet is stronger because there is more coolant injected into the mainstream. Higher momentum jets, as in the case of $M = 0.8$, can withstand higher freestream turbulence and produce similar film effectiveness levels as in the case of low freestream turbulence. For the film-cooling and S4 case, similar trends are observed, although film effectiveness values are not as high as those for the film cooling and S3 case.

Effect of Spallation Location

Figures 6b and 6c show the effect of spallation location on film effectiveness. The presence of spallation downstream of the film-cooling hole row causes the film-cooling jets to detach from the surface at the upstream edge of the spallation cavity and reattach immediately downstream. Inside the cavity, film effectiveness is lower compared to film effectiveness outside the cavity for both blowing ratios. For both blowing ratios, high film effectiveness is obtained at the upstream edge of the cavity. When the spallation is placed immediately downstream of the film-cooling hole row (S3 case), the film-cooling jets show a strong interaction with the cavity and separate almost immediately. For a low blowing ratio ($M = 0.4$), the film effectiveness values are significantly higher at the upstream edge of the spallation cavity. Immediately downstream of this edge, the film effectiveness decreases sharply.

Effect of Freestream Turbulence

Increase in turbulence intensity decreases film effectiveness for all cases. For the film-cooling only case, for $Tu = 7.1\%$, film effectiveness is significantly lower compared to film effectiveness for the low-turbulence case. For the S3 case, under high freestream turbulence ($Tu = 7.1\%$), at a low blowing ratio ($M = 0.4$) film effectiveness decreases significantly compared to the low freestream turbulence ($Tu = 1\%$) case. This could be because film-cooling jets are quickly dissipated by the oncoming mainstream flow. For higher blowing ratio, however, there is a significant increase in the film effectiveness under high-turbulence ($Tu = 7.1\%$) compared to low-turbulence ($Tu = 1\%$) conditions. Similar results are observed for the film-cooling and spallation S4 case. The film effectiveness increase for $M = 0.8$ is not as high as that for the film-cooling and spallation S3 case. Under high-turbulence conditions, in general, film effectiveness drops rapidly for low blowing ratio.

Conclusions

The effect of simulated TBC spallation on heat transfer coefficient and film effectiveness distributions over a film-cooled cylindrical leading-edge model has been studied using a transient liquid crystal image method.

In essence, the presence of a spallation downstream of film-cooling holes can provide significant changes in the way the film covers the surface. The spallation causes local flow separation and reattachment causing higher heat transfer coefficients and lower film effectiveness. The results are summarized as follows.

1) The presence of spallation causes an increase in local Nusselt numbers and causes a significant spanwise variation in film effectiveness distribution compared to a cylindrical leading-edge model with film cooling and no spallation.

2) Spallation location S3, closer to the film-cooling holes, produces a large enhancement in downstream Nusselt numbers and film effectiveness. However, spallation location S4, which is farther downstream of the film cooling holes, has very little effect on Nusselt number and film effectiveness distributions.

3) Both spallation locations cause very low film effectiveness inside the spallation cavity.

4) Freestream turbulence has very little effect on Nusselt number distributions for all cases (no spallation, spallation S3, and spallation S4). However, film effectiveness is significantly reduced at higher freestream turbulence.

5) At low freestream turbulence ($Tu = 1\%$), a lower blowing ratio ($M = 0.4$) produces higher film effectiveness. However, at higher freestream turbulence ($Tu = 7.1\%$), a higher blowing ratio ($M = 0.8$) produces higher film effectiveness.

Acknowledgments

This paper was prepared with the support of the U.S. Department of Energy, Morgantown Energy Technology Center, Cooperative Agreement DE-FC21-92 MC 9061. The support of D. B. Fant and L. P. Golan, the technical team of Advanced Gas Turbine Systems Research at Clemson University, is greatly appreciated. The authors acknowledge C. Pang Lee, of General Electric Aircraft Engines, for his valuable suggestions on this project.

References

[1]Watt, R. M., Allen, J. L., Baines, N. C., Simons, J. P., and George, M., "A Study of the Effects of Thermal Barrier Coating Surface Roughness on the Boundary Layer Characteristics of Gas Turbine Aerofoils," American Society of Mechanical Engineers, Paper 87-GT-223, June 1987.

[2]Abuaf, N., Dorri, B., Lee, C. P., and Flodman, D. A., "Stagnation Point Heat Transfer with a Thermal Barrier Coating Cylinder," American Society of Mechanical Engineers, Paper 97-GT-385, June 1997.

[3]Ekkad, S. V., and Han, J. C., "Heat Transfer Inside and Downstream of Cavities Using a Transient Liquid Crystal Method," *Journal of Thermophysics and Heat Transfer*, Vol. 10, No. 3, 1996, pp. 511–516.

[4]Ekkad, S. V., and Han, J. C., "Detailed Heat Transfer Distributions on a Cylindrical Model with Simulated TBC Spallation," *Journal of Thermophysics and Heat Transfer*, Vol. 13, No. 1, 1999, pp. 76–81.

[5]O'Brien, J. E., and Van Fossen, G. J., "The Influence of Jet-Grid Turbulence on Heat Transfer From Stagnation Region of a Cylinder in Crossflow," American Society of Mechanical Engineers, Paper 85-HT-58, Nov. 1985.

[6]Morehouse, K. A., and Simoneau, R. J., "Effect of a Rotor Wake on Local Heat Transfer on the Forward Half of a Circular Cylinder," *Proceedings of the International Heat Transfer Conference*, San Francisco, 1986, pp. 1249–1255.

[7]Bellows, W. J., and Mayle, R. E., "Heat Transfer Downstream of a Leading Edge Separation Bubble," *Journal of Turbomachinery*, Vol. 108, No. 1, 1986, pp. 131–136.

[8]Mehendale, A. B., Han, J. C., and Ou, S., "Influence of High Mainstream Turbulence on Leading Edge Heat Transfer," *Journal of Heat Transfer*, Vol. 113, No. 4, 1991, pp. 843–850.

[9]Mick, W. J., and Mayle, R. E., "Stagnation Film Cooling and Heat Transfer, Including its Effect Within the Hole Pattern," *Journal of Turbomachinery*, Vol. 110, No. 1, 1988, pp. 66–72.

[10]Mehendale, A. B., and Han, J. C., "Influence of High Mainstream Turbulence on Leading Edge Film Cooling Heat Transfer," *Journal of Turbomachinery*, Vol. 114, No. 4, 1992, pp. 707–715.

[11]Ou, S., Mehendale, A. B., and Han, J. C., "Influence of High Mainstream Turbulence on Leading Edge Film Cooling Heat Transfer: Effect of Film Hole Row Location," *Journal of Turbomachinery*, Vol. 114, No. 4, 1992, pp. 716–723.

[12]Ekkad, S. V., Han, J. C., and Du, H., "Detailed Film Cooling Measurements on a Cylindrical Leading Edge Model: Effect of Free-Stream Turbulence and Coolant Density," *Journal of Turbomachinery*, Vol. 120, No. 4, 1998, pp. 799–807.

[13]Kline, S. J., and McClintock, F. A., "Describing Uncertainties in Single Sample Experiments," *Mechanical Engineering*, Vol. 75, No. 1, 1953, pp. 3–8.